

COMPUTED TOMOGRAPHY – A NEW TOOL STUDYING HIDDEN CORROSION

Jürgen GOEBBELS, Daniel HANKE, Dietmar MEINEL, Andreas STAUDE,
Matthias BECK, Andreas BURKERT
BAM Federal Institute for Materials Research and Testing, Berlin, Germany

Abstract

Due to the progress in Computed Tomography (CT) applied for dimensional control new fields in materials characterization are opened. Especially volume properties can be non-destructively and quantitatively analysed which are non-accessible by other methods. These possibilities are used to study time dependent properties of corrosion. As an example concrete cylinders with embedded steel bars as working electrode are investigated. The mass loss of the working electrode is determined by CT and compared with results from electrochemical and gravimetric measurements. The limitations of the evaluation process of corrosion by CT are studied using a simulation program for the radiographic projections.

Introduction

The progress in Computed Tomography (CT) applied for dimensional control, which has been reached in the last years, has opened new fields in materials characterization [1]. Especially volume properties can be non-destructively and quantitatively analysed which are non-accessible by other methods. First experiments to characterize corrosion phenomena are published in [2]. This work describes time dependent properties of corrosion. As an example concrete cylinders with embedded steel bars are investigated. The used experimental set-up, the procedure to evaluate the volume of the working electrode before and after different periods of corrosion from the CT data are described and analysed. Along with the investigations by CT electrochemical methods were used to monitor corrosion of steel in concrete. Therefore the galvanostatic pulse measurement was applied to describe the continuous corrosion process on the surface of the embedded steel cylinders. Moreover the mass loss of the embedded steel cylinders was postulated from the electrochemical data using Faraday's law. Finally the results of the electrochemical studies and the results from the CT data were correlated to give a prognosis of the corrosion progress. In addition the differentiation between total and pitting corrosion is essential for the corrosion progress and first shown in these investigations non-destructively by CT.

Sample preparation

For the electrochemical investigations, mortar cylinders with embedded electrodes were produced (Fig. 1). The mortar cylinders had a height of 120 mm and a diameter of 80 mm. The concrete cylinder simulates a constant concrete cover (35 mm). In the centre of the specimen a small steel cylinder (working electrode) welded to a stainless steel filler wire is fixed. The steel cylinder had a diameter of 9 mm, a height of 10 mm and a surface of 4.1 cm². In addition to the working electrode a counter electrode (platinised titanium net) was embedded (Fig. 1). The concrete mixtures were made according to Table 1.

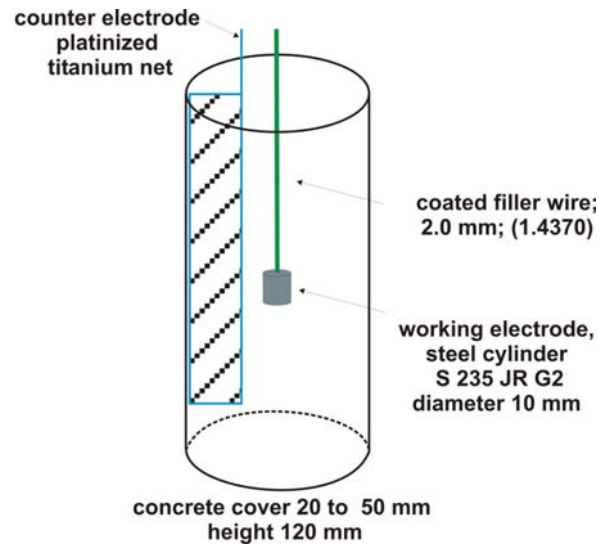


Fig. 1: Mortar (concrete) cylinder with embedded electrodes

The mortar cylinders had a height of 120 mm and a diameter of 80 mm. The concrete cylinder simulates a constant concrete cover (35 mm). In the centre of the specimen a small steel cylinder (working electrode) welded to a stainless steel filler wire is fixed. The steel cylinder had a diameter of 9 mm, a height of 10 mm and a surface of 4.1 cm². In addition to the working electrode a counter electrode (platinised titanium net) was embedded (Fig. 1). The concrete mixtures were made according to Table 1.

Table 1 shows the designation and the different parameters for the test series of the probes for studying self-corrosion. The main parameters are given by concrete composition and environmental conditions. The specimens were produced with a standard mixture („MI“- CEM I with w/b = 0.5; concrete cover 35 mm; 20°C and 85% relative humidity; 0.0; 4.0 % chloride per weight of cement).

Table 1: Parameter matrix for investigations of self-corrosion

	unit	M1 C10	M1 C14
cement content	[kg/m ³]	360	360
grading curve	[mm]	AB 8	AB 8
consistence	[cm]	45	45
binder	[-]	CEM I	CEM I
standard strength	[N/mm ²]	32.5	32.5
w/b-ratio	[-]	0.5	0.5
concrete cover	[mm]	35	35
rel. humidity	[%]	85	85
temperature	[°C]	20	20
chloride content	[M.-%/CEM]	0	4.0

In regular periods, electrochemical measurements and computed tomography were performed, to describe the advancing corrosion. After the exposure the concrete cylinders were destroyed and the steel cylinders dismantled. Finally the gravimetric mass loss of the steel cylinder was determined.

Experimental set-up for computer tomography

The versatile experimental equipment for computed tomography installed at BAM is described in [3]. Some improvements were made with respect to dimensional control with CT. Especially in connection with reference structures, calibrated by tactile measurements with coordinate measurement machines (CMM) the uncertainty of CT as a measurement tool could be decreased [4]. The measurements of the samples are performed with the 225 kV laboratory CT equipment. This consists of a 225kV micro focal X-ray tube together with a flat panel detector (Perkin Elmer XRD 1620 AM3 with a CsI scintillator screen, 2048 x 2048 elements à 200x200 μm^2). The parameters used for all measurements are 210 kV and 75 μA . As prefilter for hardening the X-ray spectra a combination of 0.5 mm Cu and 0.75 mm Ag was used. 1800 projections over 360° are measured. The integration time was 20 sec per projection. The resulting image matrix was 2011x2011x1127 voxel, with a voxel size of 45.4 μm resulting from the selected magnification of 4.4.

For the measurement only the region containing the working electrode (marked red in fig. 2) was investigated, that means a sample volume with a height of about 51 mm was sufficient.

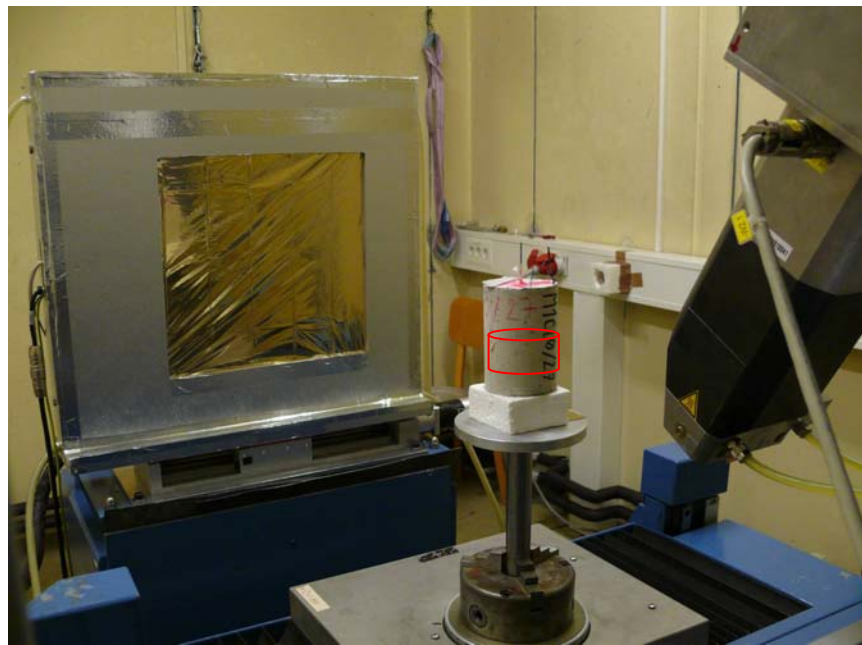


Fig. 2: CT equipment developed at BAM, with 225 kV micro focal X-ray tube, temperature stabilized flat panel detector and concrete sample. The investigated volume of the sample is marked red.

Experimental set-up for electrochemical measurements

For the electrochemical measurements the specimen and a reference electrode was positioned into a saturated calcium hydroxide solution, as shown in Figure 3. In detail the measuring device corresponds to a classical three electrode electrochemical measuring cell. For the electrochemical investigations the galvanostatic pulse technique was applied. The experimental arrangement is presented in Figure 3.

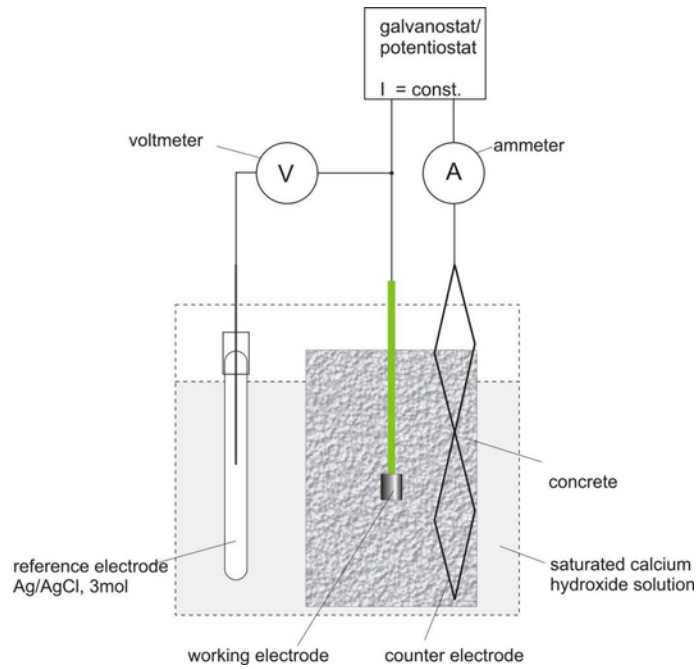


Fig. 3: Measuring device for electrochemical measurements

Four weeks after manufacturing the test series the specimens were stored under different environmental conditions as shown in Table 1. Every three months electrochemical measurements were performed and the specimens investigated by computer tomography.

During the electrochemical measurements the changes of the open circuit potentials (OCP) were documented and the polarisation resistances calculated according to Ohm's law (1). This technique of monitoring the corrosion rate has been proved previously [5-8].

$$R_p = \frac{\Delta U}{I} \quad (1)$$

R_p	polarisation resistance	[Ω]
ΔU	potential change	[V]
I	galvanostatic pulse current	[A]

From the time dependent polarisation resistances the self-corrosion current over time is calculated by using the Stern-Geary-equation (2).

$$I_{self} = B \cdot \frac{1}{R_p} \quad (2)$$

I_{self}	self-corrosion current	[A]
R_p	polarisation resistance	[Ω]
B	proportionality constant	[V]
	active: $B = 0.026$	
	passive: $B = 0.052$	

Furthermore the actual mass loss was determined, time dependent, using the self-corrosion current and different electrochemical parameters, using Faraday's law (3).

$$\Delta m_{EC} = \frac{M}{z \cdot F} \cdot I_{self} \cdot t \quad (3)$$

Δm_{EC}	mass loss determined by electrochemical data	[g]
M	molar mass	[g/mol]
t	time of outsourcing	[s]
z	number of valence electrons	[-]
F	Faraday-constant (1F = 96487 As/mol)	[As/mol]

Workflow to determine the volume of electrode and the mass loss from CT data

The workflow starts with the extraction of the volume of the electrode with the Application Software of Volume Graphics (VGStudio Max, Release 2.0). From the CT voxel data set the iso-surface of the electrode is evaluated, using the module *region growing*, which select all voxels within a tolerance band of grey values. For regions outside this grey values (ring artefacts etc.) a combination of the modules *erode/dilate* are used. Final step is the storage of this volume as ROI (Region of Interest). The stainless steel filler wire connected with the working electrode is selected by the module *polygon* and subtracted from the ROI of the electrode. This resulting ROI is the starting point for local calibration, i.e. surface determination with an adaptive threshold. The final enclosed volume is calculated with the module *volume analysis*. From the differences of the volume at different stages of deterioration the corroded volume can be calculated.

Using the current volume of the electrode, evaluated by CT data, the mass loss of electrode was determined, using the known density of steel and the mass of the specimen before pre-damaging (4).

$$\Delta m_{CT} = m_{0,grav} - (V_{steel,CT} \cdot \rho_{steel}) \quad (4)$$

Δm_{CT}	mass loss determined with data from X-ray computed tomography (CT)	[g]
$m_{0,grav}$	mass of specimen before pre-damaging	[g]
$V_{steel,CT}$	resulting steel volume calculated by data from CT	[cm ³]
ρ_{steel}	density of steel	[g/cm ³]

Results

Fig. 4 shows two iso-surface visualisations of an investigated sample volume. The image at left shows the outer surface of the sample and the image in the middle only both metallic electrodes. The corroded electrode of the sample M1CL4/26 in the state after 14 month is shown in the cross section (image at right) of Fig. 4. Some details at different stages are given in Fig. 5. Most of the corrosion products are found in the large void at the bottom of the electrode. The voids inside the electrode are filled with corrosion products. The void at left of the electrode shows a higher density at the surface resulting from precipitated corrosion products.

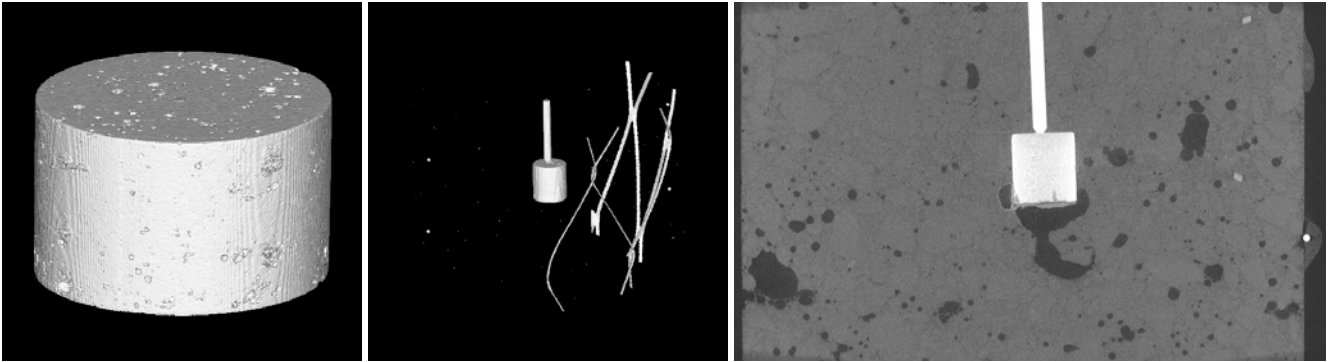


Fig. 4: Two iso-surface visualisations of the outer surface of the concrete sample (left) and the inner electrode together with the counter electrode (middle). Cross section of sample M1Cl4/26 (right).

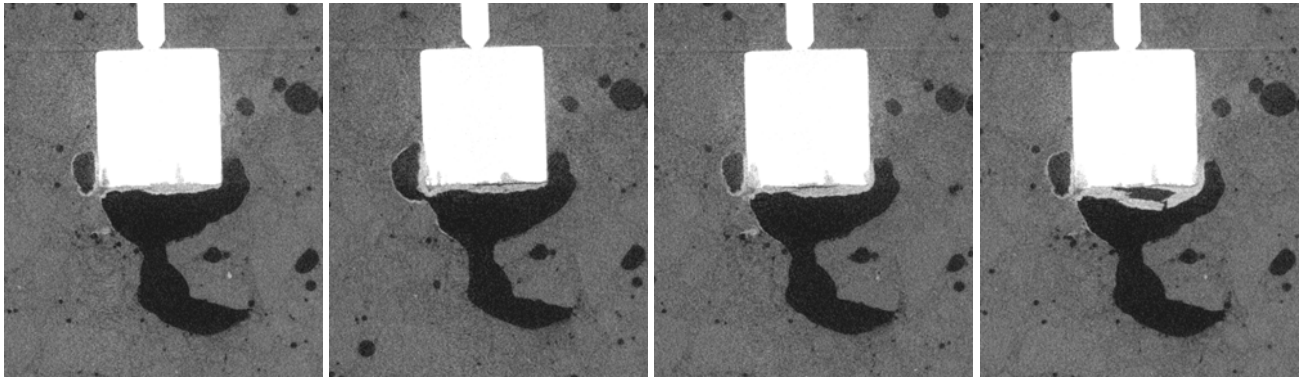


Fig. 5: Details of the electrode of sample M1Cl4/26 at different stages of self corrosion.

The volume of the electrodes calculated from CT data is shown in fig. 6 as function of time for the two sample sets M1Cl0 and M1Cl4.

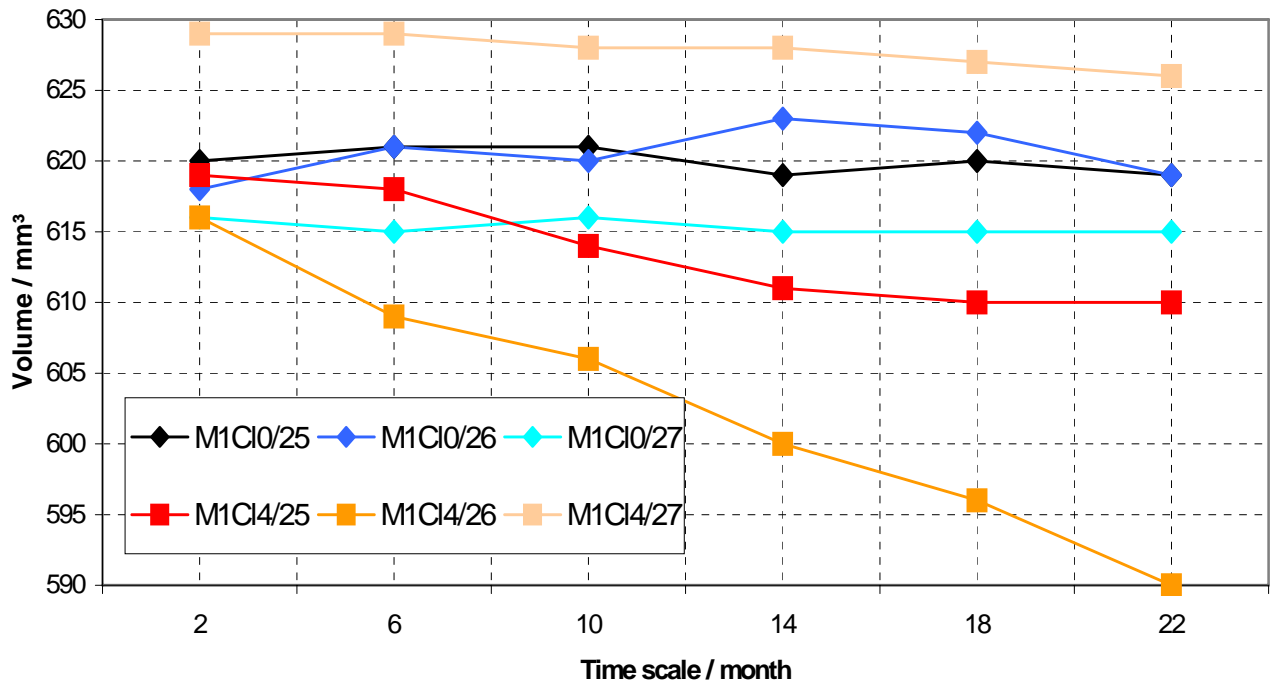


Fig. 6: Volume reduction of electrode for two sets of samples as function of time

Fig. 7 show the mass losses of all specimens, determined by computed tomography (CT), electrochemistry (EC) and the gravimetric mass loss after excavating the steel cylinder out of the concrete. It is obvious that all techniques are able to decide between active and passive specimens. The mass loss of the steel cylinders which were embedded in a chloride contaminated mortar is on a significantly higher level than that of those embedded in a pure mortar without chloride. The values show the same trends of mass losses, also the shape of the dismantled surface correlates with the mass losses like expected.

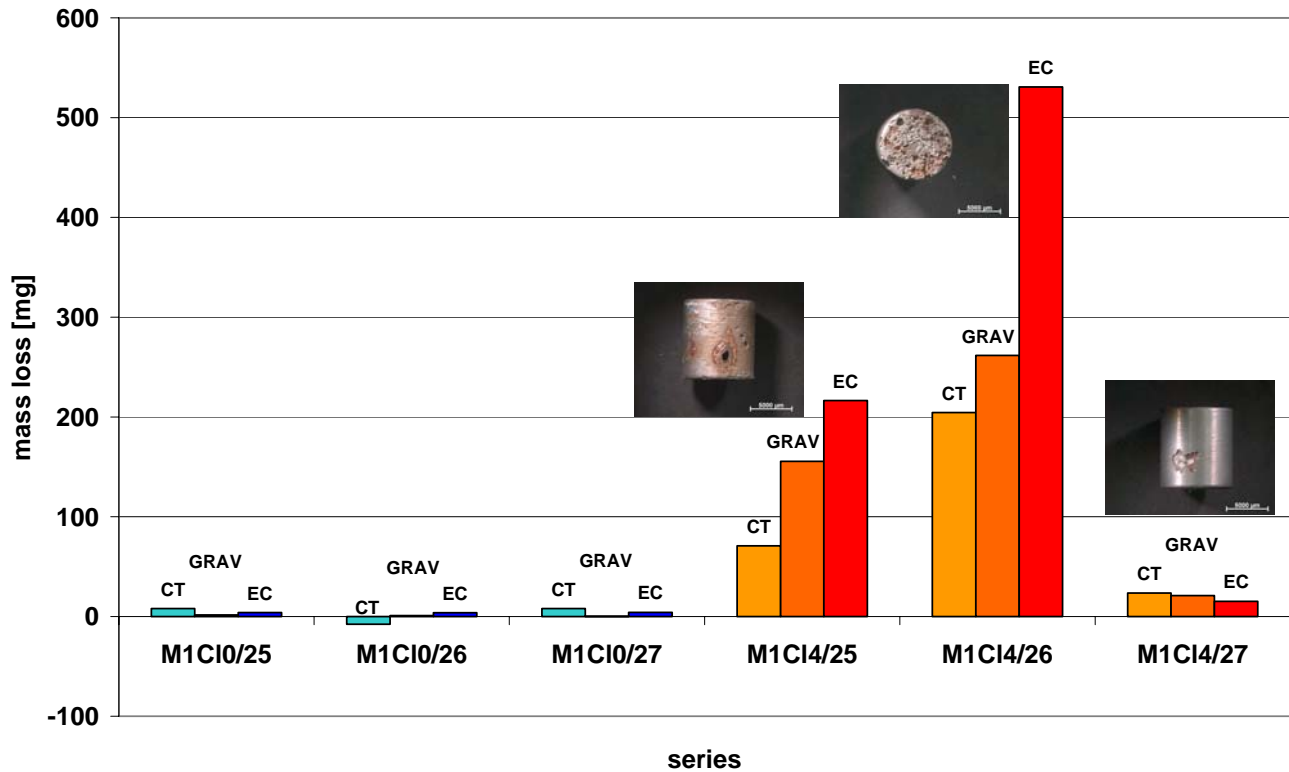


Fig. 7: Mass losses determined with data from computed tomography (CT), electrochemistry (EC) and gravimetric mass loss (GRAV)

Furthermore it is interesting to look at the details in the divergences between the mass losses. Fig. 8 shows the divergences between the gravimetric mass loss and the calculated mass losses from the data of CT and EC. It can be noticed, that the divergence between gravimetric mass loss and the calculated mass loss is very high in the case of chloride free specimens. In the case of chloride contaminated mortar with active corrosion all techniques are able to describe the real mass loss much better. Also it can be seen, that between the passive and the active specimens there is a reversal in the divergence. In the case of passive specimens the deviation CT versus GRAV is higher than EC versus GRAV, in the case of active specimens this relation reverse. If the specimens are active and the mass losses are higher in general, the deviation between CT and GRAV decreases while the divergences between EC and GRAV increase.

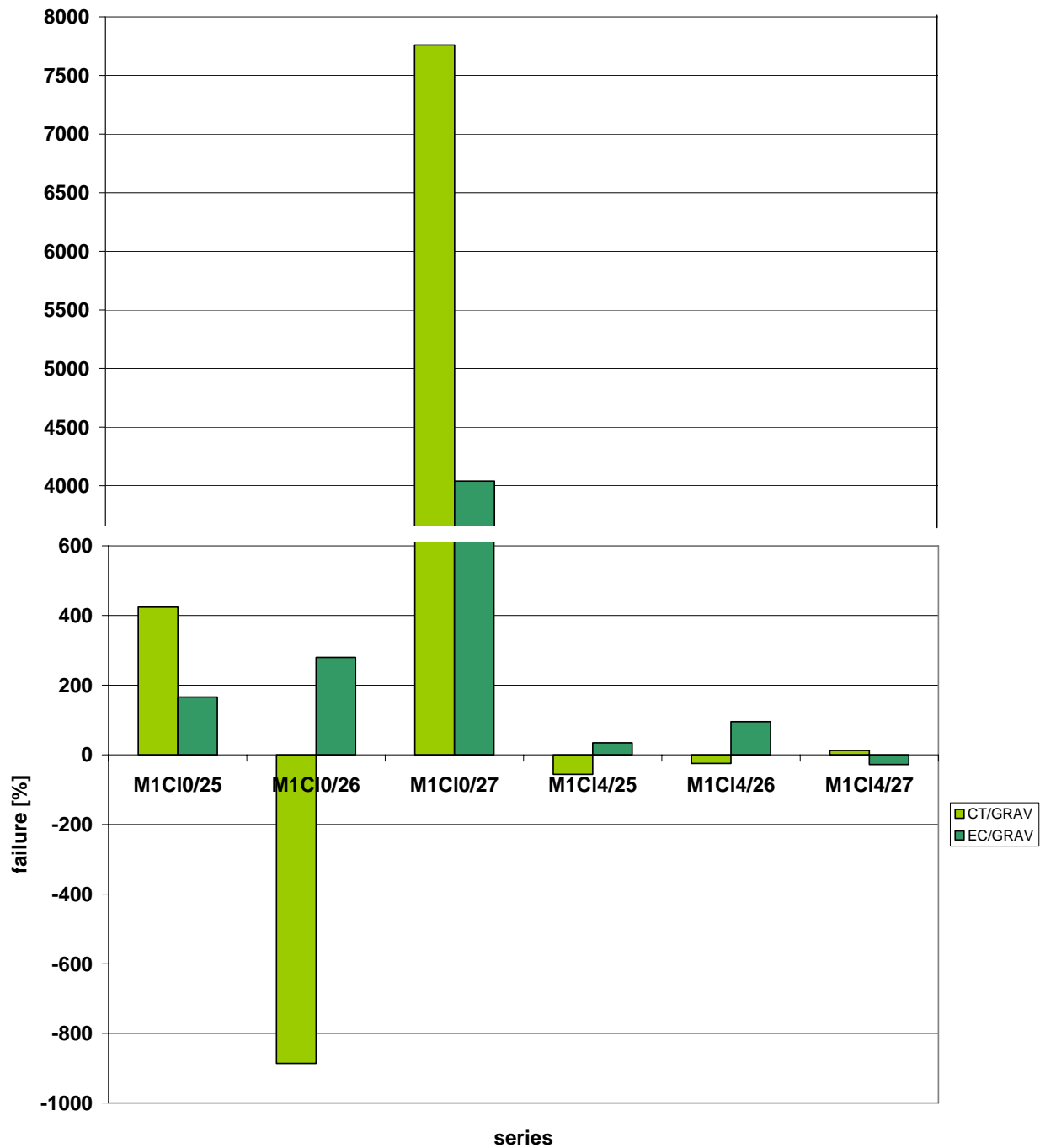


Fig. 8: Mass loss determined with data from computed tomography (CT) and electrochemistry (EC), compared to gravimetric mass loss (GRAV)

Simulation

An estimation of the detection limits of damaged areas was performed using ‘aRTist’ (analytical Radiographic Testing inspection simulation tool, developed at BAM) which has an option to simulate computed tomography measurements. The sample geometry is described by STL-data sets.

With the same parameters as used for the real measurements (X-ray parameter, detector element size, magnification, noise level) an embedded steel bar electrode was simulated with different sizes of cylindrical and conical corroded pits (Table 2). The simulation is performed under the assumption that the corroded volume is empty or filled with corrosion products with reduced density compared to the basis material of the electrode.

The nominal analytically calculated volumes of the simulated cylindrical electrode and cylindrical and conical corroded pits are in principle larger than the STL values, because the modelling of the flaws was performed (Software *Rhinoceros, Rhino 3.5*) with a limited number of triangles generating a volume which is always enclosed by the analytical model. This effect is more pronounced for the cone geometry due to the larger deviation between the circle base of the analytical model compared to the octangular base of the STL-model. The results from CT simulations show the well known effect that the volume measured by CT is in general larger than that of the input model.

Table 2: Comparison of corroded volume between analytical model, triangulated STL model and data from simulated CT.

Volume	Analytical model mm ³	STL-model mm ³	Diff. STL mm ³	CT mm ³	Diff. CT mm ³	STL vs. CT mm ³
Electrode cylinder						
Ø=9.0 mm h=10.00 mm	636.17	635.01		635.32		-0.31
Corroded cylinder						
Ø=2.0 mm h=0.040 mm	0.126	634.89	0.13	635.05	0.27	-0.16
Ø=2.0 mm h=0.080 mm	0.251	634.76	0.25	634.90	0.42	-0.14
Ø=2.0 mm h=0.160 mm	0.503	634.51	0.50	634.40	0.92	+0.11
Ø=2.0 mm h=0.320 mm	1.005	634.01	1.00	634.09	1.23	-0.08
Corroded cone						
Ø=0.125 mm h=0.625 mm	0.003	635.01	0.00	635.24	0.08	-0.23
Ø=0.250 mm h=1.250 mm	0.021	634.99	0.02	635.13	0.19	-0.14
Ø=0.500 mm h=2.500 mm	0.164	634.86	0.15	634.92	0.40	-0.06
Ø=1.000 mm h=5.000 mm	1.309	633.80	1.21	633.74	1.58	+0.06

Conclusions

From the observations in Fig. 7 and 8 it can be asserted, that CT is able to observe the ongoing corrosion of steel in concrete. In the case of passive steel cylinders the electrochemistry is able to determine the amount of corrosion much better than the CT. Nevertheless the divergence is also much higher than in the case of active systems. The basic cause is the thin passive layer of about 20-30 µm which can not be measured by CT. In this case the EC is the more applicable technique. This observation is like expected; in the case of passive systems the electrochemistry is able to describe the corrosion with limitations. The theoretic background is investigated by Heitz and Schwenck [9].

However in the case of advanced corrosion, especially pitting corrosion with deep and impenetrable pits, the CT seems to be the more dedicated technique. The corrosion promoted by hydrolysis in the pits can not be measured by the EC. In this case the investigation of corrosion by the determined steel volume is the more exact method.

References

- [1] M. Bartscher, U. Hilpert, J. Goebbels, G. Weidemann, *Enhancement and Proof of Accuracy of Industrial Computed Tomography Measurements*, CIRP Annals-Manufacturing Technology, vol. 56, issue 1 (2007)495-498.
- [2] M. Beck, J. Goebbels, A. Burkert, *Application of X-ray tomography for the verification of corrosion processes in chloride contaminated mortar*, Materials and Corrosion, 58 (2007)207-210
- [3] J. Goebbels, B. Illerhaus, Y. Onel, H. Riesemeier, G. Weidemann, *3D-Computed Tomography over Four Orders of Magnitude*, 16th World Conference on Nondestructive Testing, Montréal, Canada, August 30-September 3, (2004), CD of Proceedings
- [4] M. Bartscher, U. Hilpert, D. Fiedler, *Determination of the Measurement Uncertainty of Computed Tomography Measurements using a Cylinder Head as an Example*, tm-Technisches Messen, 75 (2008)178-186
- [5] B. Elsener, *Corrosion rate of steel in concrete-from laboratory to reinforced structures*, Materials Science Forum, 247, (1997)127-138.
- [6] J. Broomfield, K. Davies, K. Hladky, P. Noyce, *Monitoring of Reinforcement Corrosion in Concrete Structures in the Field*, Corrosion 2003, 55th Annual Conference & Exhibition, 16.-20.03.2003, San Diego, CA, USA. Houston, TX: NACE International 2003, Paper No. 03387, CD-ROM.
- [7] P. Novák, R. Malá, *Corrosion of reinforcement in concrete corrosion mechanisms and corrosion protection*, Edited by J. Mietz, R. Polder and B. Elsener, EFC Publications Number 31, IOM Communications Ltd. (2000)41.
- [8] N. Davison, G. K. Glass, A. Roberts, J. Taylor, *The Protective Effects of Electrochemical Treatment in Reinforced Concrete*, Corrosion 2003, 55th Annual Conference & Exhibition, 16.-20.03.2003, San Diego, CA, USA. Houston, TX: NACE International 2003, Paper No. 03291, CD-ROM.
- [9] E. Heitz und W. Schwenk, *Theoretische Grundlagen der Ermittlung von Korrosionsstromdichten aus Polarisationswiderständen*, Materials and Corrosion/Werkstoffe und Korrosion, 27, 4 (1976)241-245